Clinical Neurophysiology 115 (2004) 534–542

www.elsevier.com/locate/clinph

EEG minimum-norm estimation compared with MEG dipole fitting in the localization of somatosensory sources at S1

S. Komssi[a,b,c,d,e,*], J. Huttunen[a,d,e], H.J. Aronen[e], R.J. Ilmoniemi[a,e,f]

[a]*BioMag Laboratory, Engineering Centre, Helsinki University Central Hospital, P.O. Box 340, FIN-00029 HUS, Finland*
[b]*Department of Physical Sciences, University of Helsinki, P.O. Box 64, FIN-00014 University of Helsinki, Helsinki, Finland*
[c]*Department of Radiology, Helsinki University Central Hospital, P.O. Box 340, FIN-00029 HUS, Finland*
[d]*Department of Clinical Neurophysiology, Helsinki University Central Hospital, P.O. Box 340, FIN-00029 HUS, Finland*
[e]*Helsinki Brain Research Center, Helsinki, Finland*
[f]*Nexstim Ltd., Helsinki, Finland*

Accepted 30 October 2003

Abstract

Objective: Dipole models, which are frequently used in attempts to solve the electromagnetic inverse problem, require explicit a priori assumptions about the cerebral current sources. This is not the case for solutions based on minimum-norm estimates. In the present study, we evaluated the spatial accuracy of the L2 minimum-norm estimate (MNE) in realistic noise conditions by assessing its ability to localize sources of evoked responses at the primary somatosensory cortex (SI).

Methods: Multichannel somatosensory evoked potentials (SEPs) and magnetic fields (SEFs) were recorded in 5 subjects while stimulating the median and ulnar nerves at the left wrist. A Tikhonov-regularized L2-MNE, constructed on a spherical surface from the SEP signals, was compared with an equivalent current dipole (ECD) solution obtained from the SEFs.

Results: Primarily tangential current sources accounted for both SEP and SEF distributions at around 20 ms (N20/N20m) and 70 ms (P70/P70m), which deflections were chosen for comparative analysis. The distances between the locations of the maximum current densities obtained from MNE and the locations of ECDs were on the average 12–13 mm for both deflections and nerves stimulated. In accordance with the somatotopical order of SI, both the MNE and ECD tended to localize median nerve activation more laterally than ulnar nerve activation for the N20/N20m deflection. Simulation experiments further indicated that, with a proper estimate of the source depth and with a good fit of the head model, the MNE can reach a mean accuracy of 5 mm in 0.2-μV root-mean-square noise.

Conclusions: When compared with previously reported localizations based on dipole modelling of SEPs, it appears that equally accurate localization of S1 can be obtained with the MNE.

Significance: MNE can be used to verify parametric source modelling results. Having a relatively good localization accuracy and requiring minimal assumptions, the MNE may be useful for the localization of poorly known activity distributions and for tracking activity changes between brain areas as a function of time.

Keywords: Minimum-norm estimate; L2 norm; Somatosensory evoked potential; Somatosensory cortex; Spatial accuracy

1. Introduction

The task to reconstruct the current distribution underlying a measured electric or magnetic field outside the source volume is called the electromagnetic inverse problem. No unique solution exists, because a large number of source configurations is invisible to measurement sensors. This means that many current combinations may produce an identical field outside the source volume (*cf.* Ilmoniemi, 1991). The most common approach for solving the problem is the use of equivalent current dipoles (ECDs), each active brain region being modeled with at least one point-like dipole, which may be fixed in position and orientation. This approach is best suited for cases where it can be assumed that neuronal activity is localized into a small number of distinct areas of the brain.

Instead of point-like sources, some inverse algorithms search for the best estimate of a distributed primary current.

* Corresponding author. Tel.: +358-9-4718-0709; fax: +358-9-4717-6678.
E-mail address: soile.komssi@hus.fi (S. Komssi).

1388-2457/$30.00
doi:10.1016/j.clinph.2003.10.034

In minimum-norm algorithms, the solution with the smallest norm is selected from all those current distributions that could explain the measured potential or magnetic field. Requiring no a priori assumptions about the nature of the source current distribution, minimum-norm estimation (MNE) may be the best choice when the activity distribution is poorly known in advance. The MNE can be formulated in different ways (Hämäläinen and Ilmoniemi, 1984, 1994; Matsuura and Okabe, 1995; Pascual-Marqui et al., 1994; Sarvas, 1987). L2-norm solutions minimize the energy (integral of squared current density) of source currents, whereas L1-norm solutions minimize the integral of the absolute value of the source current (Matsuura and Okabe, 1995; Uutela et al., 1999). Generally, the L1 solution tends to yield more focal sources, while the L2 solution may more accurately describe distributed sources. One drawback of the L1 MNE is that its present practical solutions require prior information about current orientations, which may cause error when unknown source-current distributions are estimated. Also, the computational load is considerably higher when using the L1 norm. In realistic noise conditions, the spatial resolution of the L2 norm may even be comparable to that of the L1 norm (Fuchs et al., 1999).

The L2 MNE has been applied to several types of bioelectric and -magnetic inverse problems, such as source localization of event-related potentials and magnetic fields (Ahlfors et al., 1992; Babiloni et al., 2000; Dobel et al., 1998; Haan et al., 2000; Rinne et al., 2000; Shibata and Ioannides, 2001), multichannel magnetocardiograms (Leder et al., 1998; Numminen et al., 1995), potentials evoked by transcranial magnetic stimulation (Ilmoniemi et al., 1997; Komssi et al., 2002), and epileptic foci (Fuchs et al., 1999). However, few studies have attempted to validate the MNE localization accuracy against dipole modelling in a situation with well-characterized current sources. In the present study, we therefore wanted to evaluate the L2-norm localizations of current sources at the primary somatosensory cortex (SI), activated by median and ulnar nerve stimulation. We compared the L2-norm solutions with source localizations obtained by applying ECD modelling to somatosensory evoked magnetic fields (SEFs), as the latter method has proven to provide accurate localization of the S1 hand area (Baumgartner et al., 1991; Hari et al., 1996; Hoshiyama et al., 1996). We further tested whether the L2-norm solutions could distinguish the closely located sources activated by the two nerves. Finally, with simulation experiments, we evaluated the influence of source depth and measurement noise on the MNE localization accuracy.

2. Methods

2.1. Computation of the MNE

Any current configuration can be considered a vector in a linear current space indexed by all points of a 3-dimensional source space and by 3 orthogonal directions at each point. Those currents that contribute to a measured electroencephalogram (EEG) lie in the subspace spanned by the lead fields $\mathbf{L}$ of the N electrode derivations (e.g., pairs formed by scalp electrodes and the reference electrode). The current estimate $\hat{\mathbf{J}}$ is in this subspace and can be written in the form

$$\hat{\mathbf{J}} = \mathbf{w}^{\mathrm{T}}\mathbf{L}, \tag{1}$$

where $\mathbf{L} = [\mathbf{L}_1, \mathbf{L}_2, \ldots, \mathbf{L}_N]^{\mathrm{T}}$; $\mathbf{w} = [w_1, w_2, \ldots, w_N]^{\mathrm{T}}$ represents the weighting factors which are calculated on the basis of the measurement. Each EEG signal V_i provides a projection of the current vector on the lead field of the electrode derivation and is written as the inner product of the lead field and the primary current $\mathbf{J}^{\mathrm{p}}$ (Hämäläinen and Ilmoniemi, 1994):

$$V_i = \langle \mathbf{L}_i, \mathbf{J}^{\mathrm{p}} \rangle. \tag{2}$$

By inserting the current estimate from Eq. (1) to (2), we get a group of equations

$$\mathbf{V} = \mathbf{K}\mathbf{w} \Rightarrow \mathbf{w} = \mathbf{K}^{-1}\mathbf{V}, \tag{3}$$

where $\mathbf{K}$ is an $N \times N$ matrix containing the inner products of the lead fields. If $\mathbf{K}$ is singular, as it may be in practical measurement set-ups, its inverse does not exist, but a more general pseudoinverse $\mathbf{K}^* = (\mathbf{K}^{\mathrm{T}}\mathbf{K})^{-1}\mathbf{K}^{\mathrm{T}}$ can be calculated using the singular-value decomposition. In the Tikhonov-regularized pseudoinverse $\mathbf{K}_{\mathrm{reg}}^*$, $\mathbf{K}^{\mathrm{T}}\mathbf{K}$ is replaced with an approximating matrix $\mathbf{K}^{\mathrm{T}}\mathbf{K} + \alpha\mathbf{I}$ ($\alpha > 0$) to stabilize the solution (Tikhonov and Arsenin, 1977). The regularized MNE is finally

$$\hat{\mathbf{J}} = (\mathbf{K}_{\mathrm{reg}}^{*}\mathbf{V})^{\mathrm{T}}\mathbf{L}. \tag{4}$$

2.2. EEG and magnetoencephalographic (MEG) recording, magnetic resonance imaging

Two males (22 and 36 years) and 3 females (27, 27, and 31 years) volunteered for the study, which was approved by the ethical committee of the Department of Radiology, Helsinki University Central Hospital. The subjects were first imaged with a 1.5-T magnetic resonance imaging (MRI) scanner (Magnetom Vision, Siemens Medical Systems, Erlangen, Germany). A 3D magnetization-prepared rapid-gradient-echo sequence was used for imaging the whole head (180 sagittal slices with 1-mm thickness without gap, TR = 9.7 ms, TE = 4 ms, TI = 20 ms, flip angle 12 degrees, FOV 256 mm, matrix size 256 × 256).

SEFs were recorded with a 306-channel whole-head array consisting of 102 magnetometers and 204 planar gradiometers (VectorView, Elekta Neuromag, Helsinki, Finland). Somatosensory evoked potentials (SEPs) were simultaneously measured with a 60-channel electrode cap (Virtanen et al., 1996), with an interelectrode spacing of about 34 mm in the anteroposterior and 41 mm in

the mediolateral direction. The reference electrode was at the nose. The positions of the electrodes, the preauricular points, and the nasion were determined individually with a 3D-digitizer (Polhemus, Colchester, VT, USA) before the recording. The median and ulnar nerves at the left wrist were alternately stimulated with rectangular current pulses (duration 0.2 ms) at an interstimulus interval (ISI) of 200 ms. A short ISI was chosen to enable averaging a large number of sweeps in a relatively short period of time, and thus ensuring a good signal-to-noise ratio. Stimulus intensities were adjusted individually so that a clear twitch was seen in the abductor pollicis brevis and abductor digiti minimi muscles. Horizontal and vertical electro-oculograms were recorded. The EEG and MEG signals were bandpass filtered between 1 and 330 Hz and sampled at 1002 Hz. Sweeps containing MEG amplitudes higher than 3 pT/cm or electro-ocular or muscle artifacts exceeding 150 μV were rejected online. For both nerves, 2000 artifact-free epochs from 50 ms pre- to 100 ms poststimulus were averaged. During the measurement, the subject sat comfortably in a magnetically shielded room, with eyes closed and the head supported with pillows to avoid head movements or muscle tension at the neck.

2.3. EEG and MEG data analysis

A digital finite-impulse-response filter was applied to the averaged SEPs, with a passband of 10–100 Hz, and to the SEFs with an individually selected bandwidth with a passband of at least 25–330 Hz. For each subject, the EEG noise level was estimated from the signals by calculating the root-mean-square (RMS) amplitude during the 50-ms prestimulus period.

For constructing the MNE on the basis of the SEPs, we used a spherical volume conductor as the head model, with 4 concentric layers having homogeneous and isotropic conductivities (scalp: thickness $a = 4$ mm, conductivity $\sigma = 0.33\ \mathrm{m}^{-1}\ \Omega^{-1}$; skull: $a = 6$ mm, $\sigma = 0.0042\ \mathrm{m}^{-1}\ \Omega^{-1}$; cerebrospinal fluid: $a = 2$ mm, $\sigma = 1.0\ \mathrm{m}^{-1}\ \Omega^{-1}$; and brain: $\sigma = 0.33\ \mathrm{m}^{-1}\ \Omega^{-1}$; Peters and de Munck, 1990). The outermost sphere (scalp) was fitted to the individual electrode locations, using the least-squares algorithm. After fitting, the electrode locations were projected to the sphere surface (scalp). An individual Cartesian coordinate system was initially defined for each subject so that the *x*-axis pointed from left to right along the line connecting the preauricular points, the *y*-axis anteriorly through the nasion, and the *z*-axis upwards. The origin of the coordinate system was then transferred without rotation to the center of the individual head model; the source locations were expressed in this frame.

The MNE solution was computed on a spherical surface using Tikhonov regularization (Tikhonov and Arsenin, 1977). The regularization parameter of 10^{-5} was chosen, because it was found to result in a reasonable solution as a compromise between dispersion of the source and noise effects. Because sources at S1 usually lie at the depth of 2–4 cm below the scalp, the average being approximately at 3 cm (Buchner et al., 1995; Rossini et al., 1989; Sutherling et al., 1988), the MNE computation surface was placed 32 mm below the outermost (20 mm below the innermost) sphere surface. The surface consisted of 4096 square grid cells, each of them being occupied by 3 dipole components in orthogonal directions. For the estimation of 3-dimensional current density, the grid cells were ascribed a depth of 5 mm. This thickness was chosen to represent the part of the sulcal wall that extends below the computation layer. The MNE was calculated in 1-ms steps from 0 to 100 ms poststimulus. The position and strength of each current-density maximum was registered; these positions were used to denote the site of maximum activation, and compared with the ECD locations.

In MEG, dipolar field patterns were searched around the contralateral S1 (S1c) during 0–100 ms poststimulus, and, when found, an ECD was fitted to a subset of 22 gradiometer signals containing both extrema of the field pattern. The fitting was performed sequentially, covering 10 ms around the peaking of the dipolar field, and the source was determined by selecting the strongest dipole with a goodness-of-fit value over 80%. The innermost sphere of the 4-layer model for the MNE computation was also used as the head model for localizing the ECDs. This was done to exclude the influence of the head model on the differences between the MNE and ECD localizations.

The ECD and MNE localizations were visualized by inserting the sources into the frame of an individual anatomical 3D MRI set. The co-registration of the source positions and anatomical structures was performed individually based on the coordinates of the preauricular points and the nasion.

Because the ECDs fitted to SEFs were chosen as reference to which the MNEs were compared, we concentrated on the mainly tangential components of the somatosensory responses. With the presently used ISI and filter setting, these occurred at 20 ms (N20/N20m) and approximately 70 ms (P70/P70m) poststimulus. At latencies between 25 and 55 ms, a mixture of tangential and radial currents was active, and this period was not analyzed in detail.

2.4. Computational analysis

In the simulations (performed with MATLAB; The Mathworks, Inc., Natick, MA, USA), the MNE was constructed for a 20-nAm tangential dipole at 3 different locations and 8 different orientations at each location. Regularization parameters 10^{-6}, 10^{-5}, 10^{-4}, and 10^{-3} were used. The influence of source depth deviating from the depth of the MNE computation surface was tested with a dipole at the depths of 0, 3, 10, and 20 mm below the computation surface. The simulations were carried out in a noiseless

situation and with spatially uncorrelated noise added to the potentials.

If the outer sphere of the head model does not estimate the head shape adequately, i.e. the fitted electrode locations deviate much from their original sites, the localization is not accurate. The influence of the shifts of the electrode positions on the MNE localization accuracy was tested with one simulated dipole at 6 different locations at the surface of the innermost sphere (brain). The potential of each dipole was calculated at the digitized electrode positions of Subject 1, and the MNE was constructed after fitting the electrodes to the outermost sphere of the head model. The MNE localization was then compared with the original dipole location.

3. Results

3.1. SEP and SEF waveforms and spatial distributions

Fig. 1 shows SEPs and SEFs to left median nerve stimulation for Subject 5. The SEPs evoked by stimulation of both median and ulnar nerves consisted of parietal N20-P27-N60-P70 and frontal P20-N27-P60-N70 deflections, which were associated with dipolar field patterns reversing polarity near the central sulcus over the S1c hand area. In addition, central N35 ($n = 2$) and P45 deflections without polarity reversals and a single potential maximum over S1c were identified. Because these deflections dominated usually at 25–55 ms, clearly dipolar distributions with polarity reversal over S1c were confined to the N20 and P70 deflections; these were therefore taken to represent primarily tangential current sources at S1c. The MNE solutions showed distinct peaks in the current density values at 22, 27, 40, 48, and 67 ms poststimulus, corresponding to the N20, P27, N35, P45, and P70 deflections, respectively. Fig. 2 illustrates the potential maps and the MNEs at the peak latencies for Subject 1. The sulcal source-estimate current densities were 0.51–2.68 mA/m^2 (Table 1).

The SEFs consisted of 5 sequentially activated field patterns, peaking on the average at 21, 27, 35, 52 and 67 ms poststimulus. Each of these peaks showed a dipolar field distribution with a tangential ECD at the S1c area. Coincident tangential patterns in both MEG and EEG occurred thus at around 20 ms and around 70 ms; we designate the corresponding deflections N20/N20m and P70/P70m, respectively. These were chosen for comparisons between MNE and ECD source localizations.

The distances between the MNE and ECD localizations were 12 ± 4 (median nerve; range 8–18 mm) and 13 ± 6 mm (ulnar nerve; range 8–21 mm), for the N20/N20m deflection, and 13 ± 5 (median nerve; range 9–22 mm) and 13 ± 5 mm (ulnar nerve; range 5–17 mm), for the P70/P70m deflection. In the anatomic

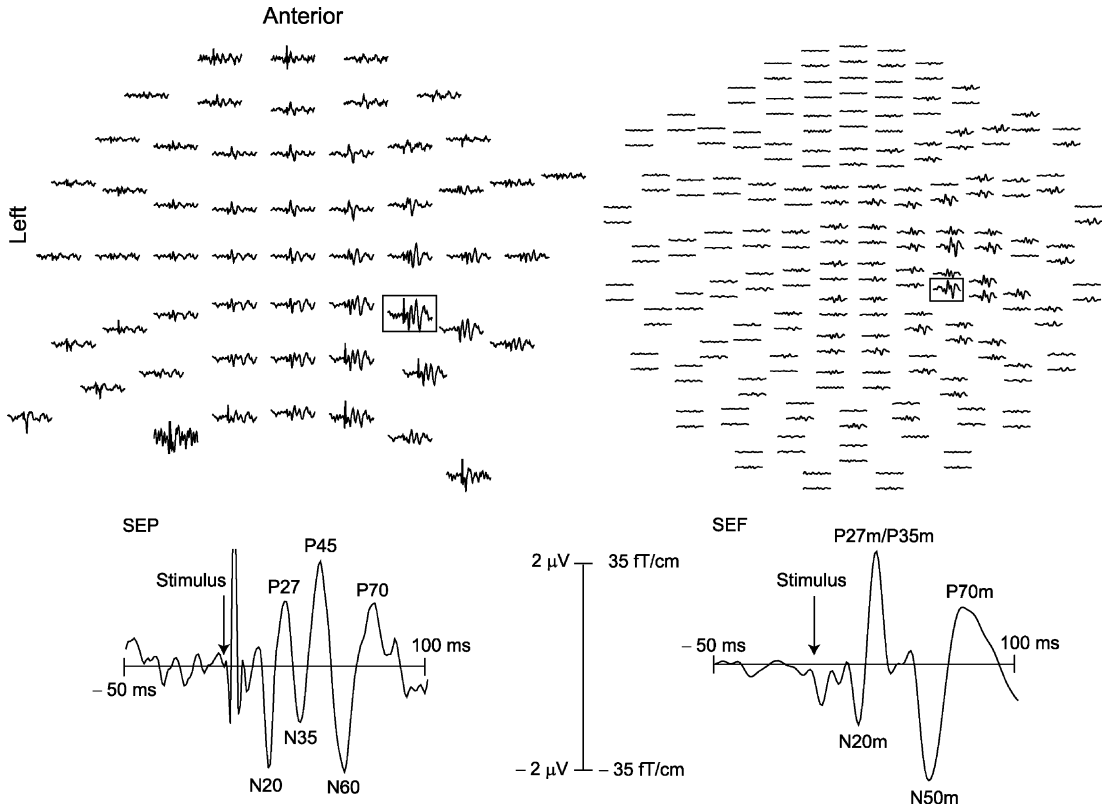

Fig. 1. Simultaneously recorded SEPs (left; 3 noisy channels are not shown) and SEFs (right; only gradiometer signals are shown) following left median nerve stimulation in Subject 5. The maximum signals over the right S1are shown enlarged.

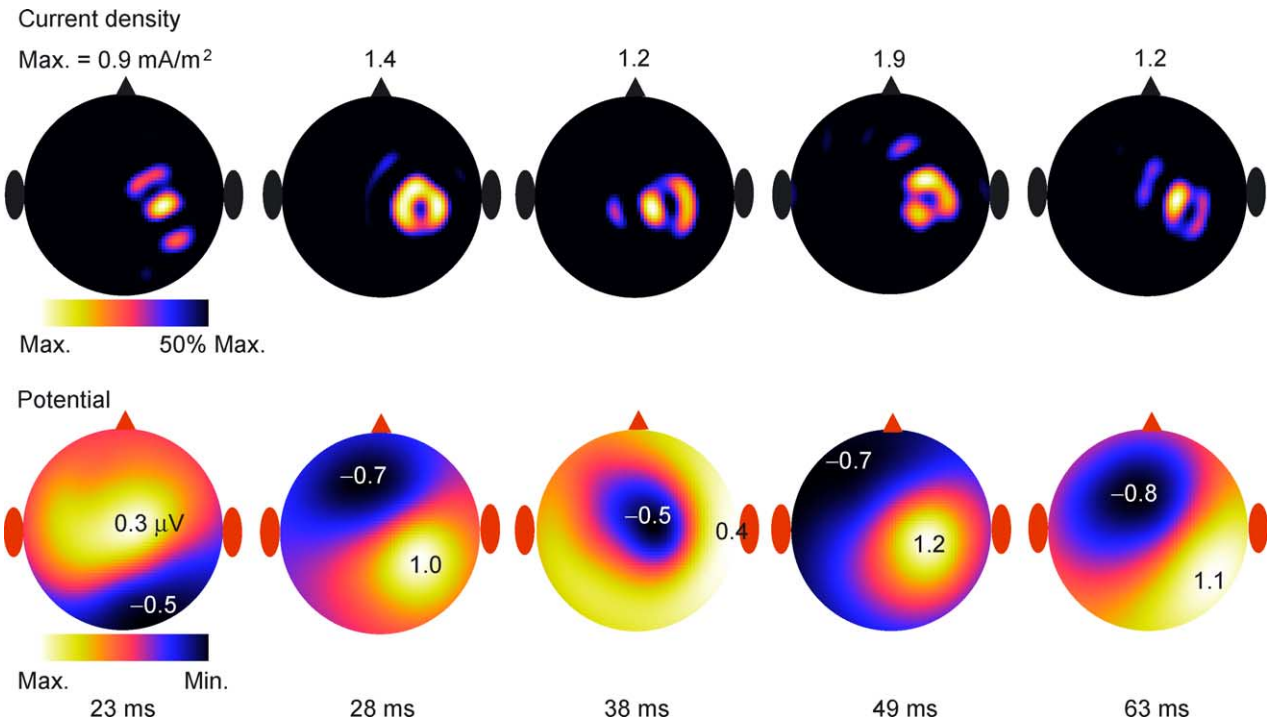

Fig. 2. MNE current-density (above) and potential (below) distributions at peak latencies 23–63 ms in Subject 1. The head is viewed from above with the nose pointing up. Note that only current density above 50% of its maximum was color-coded; the maximum value is given in each image.

MRIs, the MNE sources fell within an area between the pre- and postcentral sulcus. Fig. 3 visualizes the source localizations with respect to the individual anatomy in Subject 1.

There was a slight systematic mediolateral difference (mean 4 mm) between the ECD and MNE locations so that the ECDs were more laterally located than the MNEs (t test: $P = 0.02$; see mean source locations in Fig. 4). The ECD localized the sources approximately to the depth of the MNE computation surface (t test: $P > 0.05$); the absolute difference between the depth of the MNE and ECD sources was, however, 6 ± 1 mm. If the depth differences were omitted, the distances between corresponding MNEs and ECDs were reduced by 2–3 mm.

Fig. 4 illustrates the individual source positions for the N20/N20m and P70/P70m deflections in the mediolateral (x) and anteroposterior (y) directions. It is seen that, with the ECD, the sources for the N20/N20m deflection after median nerve stimulation were localized lateral to those after ulnar nerve stimulation (3–8 mm) for 4 of the 5 subjects, and in one medial to it (S_1, 4 mm). With the MNE, a similar mediolateral difference (5–10 mm) was seen in 3 of the 4 subjects for whom the N20 source for ulnar nerve could be localized.

For the P70/P70m deflection, the ECD tended to localize the sources for median nerve stimulation anterior (0–12 mm) and lateral (1–10 mm; in S_3, 10 mm medial) to those for ulnar nerve stimulation. Determined with the MNE, the median nerve representation was anterior (4 mm) and lateral (2 and 9 mm) to the ulnar nerve representation in two subjects, medial to it in one subject (S_1, 12 mm), and identical with it in another subject (S_2). In one subject (S_4), the MNE again failed to localize the source for ulnar nerve stimulation.

Using either the ECD or the MNE, there were no systematic differences between the N20/N20m and the P70/70m localizations.

3.2. Computational estimation of the accuracy of the MNE

In the simulation of a 20-nAm tangential dipole at the cortical surface with various locations and orientations, Tikhonov regularization of the MNE with the parameter 10^{-5} led to a source localization error of 4 ± 1 mm in a noiseless situation; this error was approximately the resolution of the computation grid, which ultimately restricted the localization accuracy. When Gaussian

Table 1
Source peak latencies (t) and strengths for the N20/N20m and the P70/P70m responses (mean ± SD (range))

Nerve	MNE		ECD	
	t (ms)	J_{max} (mA/m^2)	t (ms)	Q (nAm)
Median	22 ± 2 (21–24)	1.4 ± 0.8	21 ± 1 (20–22)	9.7 ± 2.6
Median	67 ± 6 (59–74)	1.3 ± 1.0	66 ± 8 (54–75)	6.9 ± 4.8
Ulnar	22 ± 2 (20–23)	1.3 ± 0.4	21 ± 1 (20–23)	7.4 ± 3.7
Ulnar	67 ± 5 (60–72)	1.5 ± 0.6	64 ± 8 (53–72)	6.7 ± 9.3

J_{max} is the MNE current-density maximum and Q is the dipole moment of the ECD.

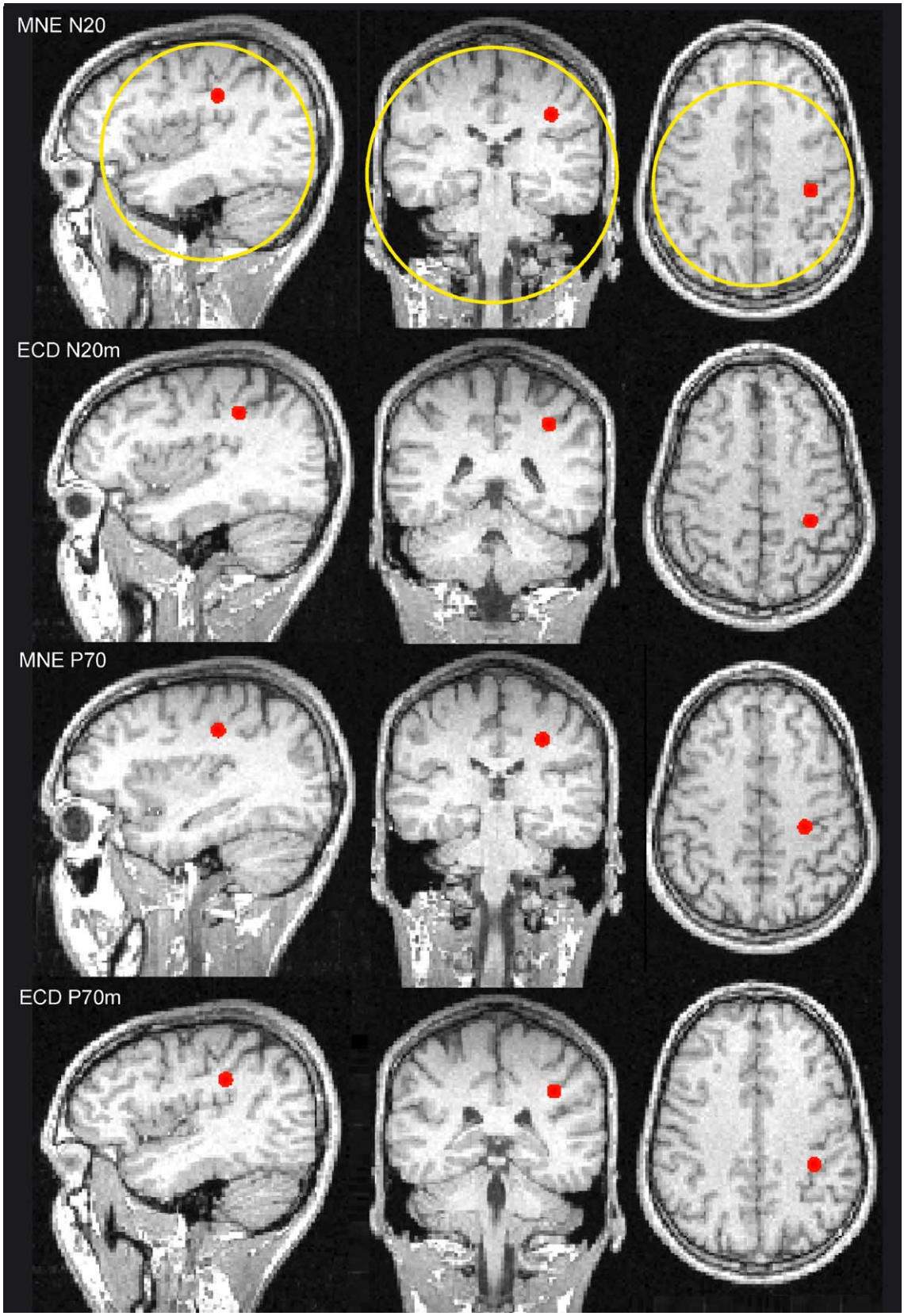

Fig. 3. MNE and ECD source localizations for the N20/N20m and the P70/P70m deflections after median nerve stimulation in Subject 1, shown with respect to the individual anatomy. The MNE peaked at 23 and 63 ms, and the ECDs were best fitted at 22 and 69 ms. The distance between the MNE and ECD localizations was 10 and 9 mm for the N20/N20m and the P70/P70m responses, respectively. The yellow circle indicates the cortical surface in the head model, lying 20 mm above the spherical computation layer for the MNE.

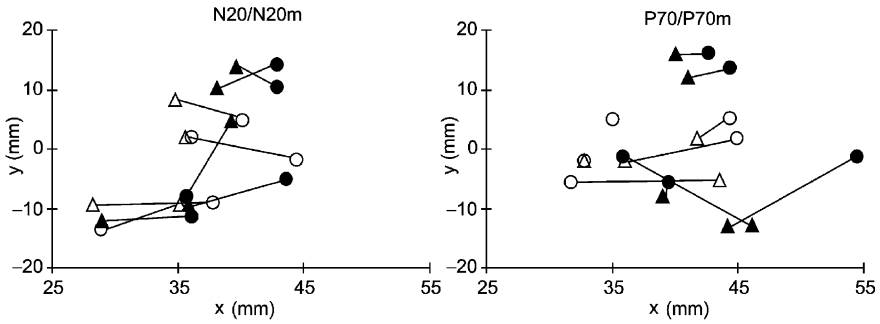

	ECD		MNE	
	N20m	P70m	N20	P70
Median n.	● $x = 40 \pm 4$; $y = 0 \pm 12$	$x = 43 \pm 7$; $y = 4 \pm 10$	○ $x = 37 \pm 6$; $y = -4 \pm 8$	$x = 38 \pm 6$; $y = 1 \pm 5$
Ulnar n.	▲ $x = 36 \pm 4$; $y = 1 \pm 12$	$x = 42 \pm 3$; $y = -1 \pm 14$	△ $x = 34 \pm 4$; $y = -2 \pm 9$	$x = 39 \pm 5$; $y = -2 \pm 3$

Fig. 4. Individual *x*- and *y*-coordinates for the MNE (↓ median nerve; ↖ ulnar nerve) and ECD (○ median nerve; △ ulnar nerve) source localizations for the N20/N20m and the P70/P70m responses; the mean locations (± SD) are given below. The lines connect source locations for median and ulnar nerve stimulation for each subject, deflection, and localization method. The origin of the Cartesian coordinate system was at the center of the head model, *x*-axis pointing to the right and *y*-axis in the anterior direction.

noise, with the same RMS amplitude (0.2 μV) as in the averaged SEPs, was added to the potential, the MNE localized the source 5 ± 3 mm from its actual position. With the regularization parameters 10^{-3} and 10^{-4}, allowing a relatively wide source distribution, the average localization error was not changed, being 5 ± 2 mm for both. The parameter 10^{-6} resulted in an average mislocalization of 14 mm, because more noise was picked up.

A dipole positioned at the depth of 3 mm below the MNE computation surface led to a mislocalization of 7 ± 4 mm (regularization parameter 10^{-5}). At 10 mm below the computation surface, the dipole was localized 15 ± 8 mm (regularization parameter 10^{-4}) from its actual location. At the depth of 20 mm below the computation surface, localization of the source did not succeed.

In one subject (S_3), the potentials of superficial 20-nAm tangential dipoles placed at 6 different locations around the sensorimotor cortex were calculated at the digitized electrode locations. The electrode locations were then fitted to the surface of the spherical model prior to the calculation of the lead fields. The mean distance between the digitized and fitted electrode locations was 11.5 mm. In this situation, the MNE localized the sources at 10 ± 6 mm from the original dipole positions.

4. Discussion

We evaluated the accuracy of the L2-minimum-norm estimation in the localization of activity at S1 measured with multichannel EEG. No a priori knowledge about the source location was introduced, apart from restricting the source to a certain depth. Compared with ECD locations obtained from SEFs, a mean localization accuracy of 13 mm was reached in 0.2-μV RMS noise. In addition to locating the S1c hand area, the MNE reconstruction allowed us also to separate the sources activated by the median nerve from those activated by the ulnar nerve stimulation with an accuracy approximately comparable to that of the ECDs derived from SEFs. Simulations together with the measured data indicated that, with a proper estimate of the source depth and with a good fit of the head model, a 5-mm mean accuracy can be reached.

We chose to focus on SEPs from S1c, because their generators are relatively well known from EEG and MEG studies (Allison et al., 1989, 1991a,b; Buchner et al., 1996; Deiber et al., 1986; Desmedt and Bourguet, 1985; Desmedt and Tomberg, 1989; Goff et al., 1977; Huttunen et al., 1987; Jones and Power, 1984; Kawamura et al., 1996; Maccabee et al., 1983; Mauguière et al., 1983; Rossini et al., 1989; Sutherling et al., 1988; Tiihonen et al., 1989; Wikström et al., 1996; Wood et al., 1985). We analyzed the N20/N20m and P70/P70m deflections, as these were explained by mainly tangentially oriented currents and were thus detectable both in EEG and MEG. We used high-pass filtering with relatively high cut-off frequencies to ensure a good signal-to-noise ratio; this affected the SEP waveform configuration so that the individual peak latencies were somewhat different from those usually found in the literature.

Because of the curved course of the central sulcus at the hand region of S1 and the somatotopic organization of this area, the cortical representation for the ulnar nerve is usually located more medially and slightly more posteriorly than that for the median nerve (Penfield and Jasper, 1954). In our study, the difference of these representations was demonstrated in the mediolateral direction for the N20/N20m, and

in both the mediolateral and anteroposterior direction for the P70/P70m. In essence, the MNE appeared equally accurate compared with the ECD in separating the closely spaced sources corresponding to ulnar and median nerves from each other.

In one previous study, ECD locations derived from scalp-recorded SEPs were compared with localizations obtained from electrocorticography; a mean distance of 8 mm was found (Sutherling et al., 1988). Some studies have applied spatiotemporal forward modelling (BESA; Megis Software, Inc., Germany) to scalp-recorded SEPs. In the study of Buchner et al. (1995), comparison with the electrocorticogram yielded a distance less than 9 mm from the central sulcus. These authors also found a mean localization difference of 6 mm between two serial recordings. In an oddball somatosensory paradigm, an average interoperator difference of 14 mm in dipole locations was found with BESA (Miltner et al., 1994). Thus, our MNE accuracies were comparable to those determined previously with dipole modelling methods applied to SEP data.

In the simulations we assessed the effects of two sources of localization error, which were likely to account for the most part of the MNE localization inaccuracy. The first source of error was the inadequacy of the spherical head model. To derive the MNE from the scalp EEG, the digitized electrode locations were first fitted to the outermost sphere of the 4-layer head model. The lead fields, which depend on the electrode locations with respect to the source space, were calculated after this fitting. The consequent shift in the electrode positions, reflecting the insuffiency of the sphere in the estimation of the head shape, obviously affected the lead fields. We showed that the MNE localization error due to the head model was on the order of 10 mm; hence, the use of realistic head models could significantly improve localization accuracy. Another potential source of mislocalization related to the head model lies in the conductivity values used for the different tissues. Our head model was based on the widely used conductivity values reported by Peters and de Munck (1990). Yet, the estimates on the conductivity of different head tissues, especially of the skull, may vary by a factor of up to 5 (Ferree et al., 2000; Oostendorp et al., 2000).

A second significant source of localization inaccuracy was the use of a spherical surface as the computation space for the MNE solutions. Instead of a 3 dimensional space, a 2-dimensional surface was chosen in order to limit the computational load of the inverse calculation. The 4096-point grid at the preset depth of 20 mm below the innermost sphere of the head model was adopted to represent the neocortical surface. This is clearly an oversimplification of the folded cortical structure and necessarily introduces errors when locating sources with a depth significantly different from 20 mm. We showed with the simulations that even relatively small deviations of the actual source depth from 20 mm led to slight mislocalization of the source also in tangential directions. An improved localization might be achieved by calculating the MNE in a 3-dimensional space. Then, however, the solution would tend to overemphasize superficial sources at the cost of deep ones. There have been attempts to overcome this problem by normalizing the lead fields to account for the depth effect (i.e. weighting the MNE solution). With a weighted MNE and a realistic head model, an accuracy of 8 mm has been attained (Babiloni et al., 2000). The accuracy of the MNE solution might be further improved, e.g., by repetitive calculation of the current, dropping out the grid points with the smallest current densities at each calculation step and, in this way, searching the active brain areas iteratively (Gorodnitsky et al., 1995; Srebro, 1996). Laplacian transformation of EEG prior to the inverse calculation has also been suggested (Babiloni et al., 2000).

We conclude that the S1 hand area can be reasonably well localized by applying the L2-MNE on scalp recorded SEPs. In future studies, utilization of realistic head models and a 3-dimensional computation space may increase MNE localization accuracy.

Acknowledgements

The work was supported by grants from the Academy of Finland, the Radiology Society of Finland, the Cancer Organizations of Finland, the Jusélius Foundation, the Instrumentarium Science Foundation, the Paulo Foundation, Helsinki University Central Hospital funds (projects TYH-9307, TYH-0313), and the Nordic Cancer Union. The authors thank Dr Sauli Savolainen for valuable comments on the manuscript.

References

Ahlfors SP, Ilmoniemi RJ, Hämäläinen MS. Estimates of visually evoked cortical currents. Electroenceph clin Neurophysiol 1992;82:225–36.

Allison T, McCarthy G, Wood CC, Darcey TM, Spencer DD, Williamson PD. Human cortical potentials evoked by stimulation of the median nerve. I. Cytoarchitectonic areas generating short-latency activity. J Neurophysiol 1989;62:694–710.

Allison T, McCarthy G, Wood CC, Jones SJ. Potentials evoked in human and monkey cerebral cortex by stimulation of the median nerve. Brain 1991a;114:2465–503.

Allison T, Wood CC, McCarthy G, Spencer DD. Cortical somatosensory evoked potentials. II. Effects of excision of somatosensory or motor cortex in humans and monkeys. J Neurophysiol 1991b;66:64–82.

Babiloni F, Babiloni C, Locche L, Cincotti F, Rossini PM, Carducci F. High-resolution electro-encephalogram: source estimates of Laplacian-transformed somatosensory-evoked potentials using a realistic subject head model constructed from magnetic resonance images. Med Biol Eng Comput 2000;38:512–9.

Baumgartner C, Doppelbauer A, Deecke L, Barth DS, Zeitlhofer J, Lindinger G, Sutherling WW. Neuromagnetic investigation of somatotopy of human hand somatosensory cortex. Exp Brain Res 1991;87:641–8.

Buchner H, Adams L, Müller A, Ludwig I, Knepper A, Thron A, Niemann K, Scherg M. Somatotopy of human hand somatosensory cortex revealed by dipole source analysis of early somatosensory evoked

potentials and 3D-NMR tomography. Electroenceph clin Neurophysiol 1995;96:121–34.

Buchner H, Waberski TD, Fuchs M, Drenckhahn R, Wagner M, Wischmann H-A. Postcentral origin of P22: evidence from source reconstruction in a realistically shaped head model and from a patient with a postcentral lesion. Electroenceph clin Neurophysiol 1996;100:332–42.

Deiber MP, Giard MH, Mauguière F. Separate generators with distinct orientations for N20 and P22 somatosensory evoked potentials to finger stimulation. Electroenceph clin Neurophysiol 1986;65:321–34.

Desmedt JE, Bourguet M. Color imaging of parietal and frontal somatosensory potential fields evoked by stimulation of median or posterior tibial nerve in man. Electroenceph clin Neurophysiol 1985;62:1–17.

Desmedt JE, Tomberg C. Mapping early somatosensory evoked potentials in selective attention: critical evaluation of control conditions used for titrating by difference the cognitive P30, P40, P100 and N140. Electroenceph clin Neurophysiol 1989;74:321–46.

Dobel C, Hauk O, Zobel E, Eulitz C, Pulvermüller F, Cohen R, Schönle PW, Elbert T, Rockstroh B. Monitoring brain activity of human subjects during delayed matching to sample tasks comparing verbal and pictorial stimuli with modal and cross-modal presentation: an event related potential study employing a source reconstruction method. Neurosci Lett 1998;253:179–82.

Ferree TC, Eriksen KJ, Tucker DM. Regional head tissue conductivity estimation for improved EEG analysis. IEEE Trans Biomed Eng 2000; 47:1584–92.

Fuchs M, Wagner M, Köhler T, Wischmann HA. Linear and non-linear current density reconstructions. J Clin Neurophysiol 1999;16:267–95.

Goff GD, Matsumiya Y, Allison T, Goff WR. The scalp topography of human somatosensory and auditory evoked potentials. Electroenceph clin Neurophysiol 1977;42:57–76.

Gorodnitsky IF, George JS, Rao BD. Neuromagnetic source imaging with FOCUSS: a recursive weighted minimum norm algorithm. Electroenceph clin Neurophysiol 1995;95:231–51.

Haan H, Streb J, Bien S, Rosler F. Individual cortical current density reconstructions of the semantic N400 effect: using a generalized minimum norm model with different constraints (L1 and L2 norm). Hum Brain Mapp 2000;11:178–92.

Hari R, Nagamine R, Nishitani N, Mikuni N, Sato T, Tarkiainen A, Shibasaki H. Time-varying activation of different cytoarchitectonic areas of the human SI cortex after tibial nerve stimulation. NeuroImage 1996;4:111–8.

Hoshiyama M, Kakigi R, Koyama S, Kitamura Y, Shimojo M, Watanabe S. Somatosensory evoked magnetic fields following stimulation of the lip in humans. Electroenceph clin Neurophysiol 1996;100:96–104.

Huttunen J, Hari R, Leinonen L. Cerebral magnetic responses to stimulation of ulnar and median nerves. Electroenceph clin Neurophysiol 1987;66: 391–400.

Hämäläinen MS, Ilmoniemi RJ. Interpreting measured magnetic fields of the brain: estimates of current distributions. Helsinki: Helsinki University of Technology; 1984.

Hämäläinen MS, Ilmoniemi RJ. Interpreting magnetic fields of the brain: minimum norm estimates. Med Biol Eng Comput 1994;32:35–42.

Ilmoniemi RJ. Estimates of neuronal current distributions. Acta Otolaryngol Suppl 1991;491:80–7.

Ilmoniemi RJ, Virtanen J, Ruohonen J, Karhu J, Aronen HJ, Näätänen R, Katila T. Neuronal responses to magnetic stimulation reveal cortical reactivity and connectivity. NeuroReport 1997;8:3537–40.

Jones SJ, Power CN. Scalp topography of human somatosensory evoked potentials: the effect of interfering tactile stimulation applied to the hand. Electroenceph clin Neurophysiol 1984;58:25–36.

Kawamura T, Nakasato N, Seki K, Kanno A, Fujita S, Fujiwara S, Yoshimoto T. Neuromagnetic evidence of pre- and post-central cortical sources of somatosensory evoked responses. Electroenceph clin Neurophysiol 1996;100:44–50.

Komssi S, Aronen HJ, Huttunen J, Kesäniemi M, Soinne L, Nikouline VV, Ollikainen M, Roine RO, Karhu J, Savolainen S, Ilmoniemi RJ. Ipsi- and contralateral EEG reactions to transcranial magnetic stimulation. Clin Neurophysiol 2002;113:175–84.

Leder U, Pohl H-P, Michaelsen S, Fritschi T, Huck M, Eichhorn J, Müller S, Nowak H. Non-invasive biomagnetic imaging in coronary artery disease based on individual current density maps of the heart. Int J Cardiol 1998;64:83–92.

Maccabee PJ, Pinkhasov EI, Cracco RQ. Short latency somatosensory evoked potentials to median nerve stimulation: effect of low frequency filter. Electroenceph clin Neurophysiol 1983;55:34–44.

Matsuura K, Okabe Y. Selective minimum-norm solution of the biomagnetic inverse problem. IEEE Trans Biomed Eng 1995;42:608–15.

Mauguière F, Desmedt JE, Courjon J. Astereognosis and dissociated loss of frontal or parietal components of somatosensory evoked potentials in hemispheric lesions. Detailed correlations with clinical signs and computerized tomographic scanning. Brain 1983;106:271–311.

Miltner W, Braun C, Johnson R, Simpson GV, Ruchkin DS. A test of brain electrical source analysis (BESA): a simulation study. Electroenceph clin Neurophysiol 1994;91:295–310.

Numminen J, Ahlfors S, Ilmoniemi R, Montonen J, Nenonen J. Transformation of multichannel magnetocardiographic signals to standard grid form. IEEE Trans Biomed Eng 1995;42:72–8.

Oostendorp TF, Delbeke J, Stegeman DF. The conductivity of the human skull: results of in vivo and in vitro measurements. IEEE Trans Biomed Eng 2000;47:1487–92.

Pascual-Marqui RD, Michel CM, Lehmann D. Low-resolution electromagnetic tomography: a new method for localizing electrical activity in the brain. Int J Psychophysiol 1994;18:49–65.

Penfield W, Jasper H. Epilepsy and the functional anatomy of the human brain. Boston: Little, Brown and Company; 1954.

Peters M, de Munck J. On the forward and the inverse problem for EEG and MEG. In: Grandori F, Hoke M, Romani GL, editors. Auditory evoked magnetic fields and electric potentials. Basel: Karger; 1990. p. 70–102.

Rinne T, Alho K, Ilmoniemi RJ, Virtanen J, Näätänen R. Separate time behaviors of the temporal and frontal mismatch negativity sources. NeuroImage 2000;12:14–19.

Rossini PM, Narici L, Romani GL, Traversa R, Cecchi L, Cilli M, Urbano A. Short latency somatosensory evoked responses to median nerve stimulation in healthy humans: electric and magnetic recordings. Int J Neurosci 1989;46:67–76.

Sarvas J. Basic mathematical and electromagnetic concepts of the biomagnetic inverse problem. Phys Med Biol 1987;32:11–22.

Shibata T, Ioannides AA. Contribution of the human superior parietal lobule to spatial selection process: an MEG study. Brain Res 2001;897:164–8.

Srebro R. Iterative refinement of the minimum norm solution of the bioelectric inverse problem. IEEE Trans Biomed Eng 1996;43:547–52.

Sutherling WW, Crandall PH, Darcey TM, Becker DP, Levesque MF, Barth DS. The magnetic and electric fields agree with intracranial localizations of somatosensory cortex. Neurology 1988;38:1705–14.

Tiihonen J, Hari R, Hämäläinen M. Early deflections of cerebral magnetic responses to median nerve stimulation. Electroenceph clin Neurophysiol 1989;74:290–6.

Tikhonov AN, Arsenin VY. Solutions of ill-posed problems. Washington, DC: V. H. Winston & Sons; 1977.

Uutela K, Hämäläinen M, Somersalo E. Visualization of magnetoencephalographic data using minimum current estimates. Neuroimage 1999;10: 173–80

Virtanen J, Rinne T, Ilmoniemi RJ, Näätänen R. MEG-compatible multichannel EEG electrode array. Electroenceph clin Neurophysiol 1996;99:568–70.

Wikström H, Huttunen J, Korvenoja A, Virtanen J, Salonen O, Aronen H, Ilmoniemi RJ. Effects of interstimulus interval on somatosensory evoked magnetic fields (SEFs): a hypothesis concerning SEF generation at the primary sensorimotor cortex. Electroenceph clin Neurophysiol 1996;100:479–87.

Wood CC, Cohen D, Cuffin BN, Yarita M, Allison T. Electrical sources in human somatosensory cortex: identification by combined magnetic and potential recordings. Science 1985;227:1051–3.